Two-dimensional MHD simulation of the solar wind interaction with magnetic field anomalies on the surface of the Moon

Erika M. Harnett and Robert Winglee

Geophysics Program, University of Washington, Seattle

Abstract. Two-dimensional magnetohydrodynamic simulations of the solar wind interaction with the magnetized regions on the surface of the Moon suggest "mini-magnetospheres" can form around the regions on the Moon when the magnetic anomaly field strength is above 10 nT at 100 km above the surface (for a surface field strength of 290 nT) and when the solar wind ion density is below 40 cm^{-3}, with typical observations placing anomalous magnetic field strengths around 2 nT at 100 km above the surface. The results suggest that not only can a bow shock and magnetopause form around the small anomalies, but their position and shape can change dramatically with changes in the solar wind conditions. A switch from southward to northward interplanetary magnetic field (IMF) causes the size of the mini-magnetosphere to increase by 90% and the magnetic field at various positions inside the bow shock to increase by a factor of 10. In addition to affecting the stand-off distance, changes in the IMF can also cause the mini-magnetosphere to go from very round to flat and elongated. The scale size of the mini-magnetospheres is 100 km for the range of typical solar wind conditions and the surface magnetic field strengths measured by Lunar Prospector. A stagnation point inside the shock region also exists for several solar wind conditions.

1. Introduction

Lunar magnetic field measurements made during the Apollo missions provided the first suggestions that the Moon has regions of high magnetic field up to 100 km in scale size with field strengths over 300 nanotesla at the surface and of the order of 2 nT approximately 100 km above the anomalies. A discussion of the results can be found in the works of *Sharp et al.* [1973], *Dyal et al.* [1974], and *Hood et al.* [1981] with a summary in the work of *Lin et al.* [1988]. Dyal et al. compared orbital magnetometer data from Apollo missions that did not make surface field measurements with those missions that did and determined that field strengths of the order of 1000 nT may be present in some small regions.

Lunar Prospector (LP) recently finished mapping the magnetic field strengths over the entire Lunar surface using both magnetometers and electron reflection detectors, and found surface magnetic fields up to 300 nT (for $5^o \times 5^o$ resolution), on spatial scales of 7 to 1000 km [*Lin et al.*, 1998,]. The magnetized regions located near the Imbrium and Serenitatis antipodes are 1200 and 740 km (respectively) in diameter with a magnitude of the order of 300 nT for that entire region. Also seen was the indication that these localized magnetized regions can interact with the solar wind to possibly form a bow shock. This bow shock is seen in the LP data as enhancements in the magnetic fields at the satellite altitudes when compared to the same region when it was in the vacuum of the Lunar wake. In conjunction with measurements indicating a change in the shape of the electron spectrum and small changes in the angle of the magnetic field, it was concluded that the surface magnetic fields were able to cause a pile-up of the interplanetary magnetic field (IMF).

The idea of small-scale magnetospheres, or "mini-magnetospheres," was reinforced by one set of measurements showing the disappearance and reappearance of an increase in the magnetic field at the satellite altitude during successive orbits over an anomalous region. The disappearance coincided with a large increase in the dynamic pressure of the solar wind. If LP was measuring only the surface field, its presence would not be affected by the solar wind. *Lin et al.* [1998] concluded that the increase in magnetic field measured over the anomaly was the pile-up of the IMF at a shock

surface and when the dynamic pressure of the solar wind increased, the shock surface dropped below the altitude of the satellite.

Shock regions may have also been measured by the Apollo 15 and 16 satellites. *Russell and Lichtenstein* [1975] showed that the occurrence of limb compression or amplifications of the ambient magnetic field at or in front of the terminator was not correlated to the direction of the IMF but rather appeared to coincide with regions with surface magnetization. The locations that they indicated as having a high occurrence rate for limb compression are in the vicinity of the Imbrium, Serenitatis, and Oriental antipodes; all three being large regions of high surface magnetic field. Russell and Lichtenstein concluded that is was highly likely that limb compressions were caused by deflection of the solar wind by magnetic anomalies in the limb region and that the size of the compressions was controlled by direction of the IMF.

In attempt to explain the high albedo of the Lunar surface in the regions of large crustal magnetic fields, *Hood and Williams* [1989] mapped the three-dimensional (3-D) particle trajectories for single particles interacting with Lunar magnetic anomalies. Their model neglected any collective effects on the incident particles and simply looked at the deflection of single particles by the Lorentz force. An estimate of the total deflection came from combining the results for an array of single particle interactions. Hood and Williams modeled the magnetic anomalies as a collection of 9-15 buried dipoles, contained in a region 100-200 km in diameter. The total field strengths were much greater than 1000 nT at the surface and of the order of 2 nT at 100 km above the surface. Their model predicted that the magnetic anomalies could produce a measurable deflection of the solar wind. They found that for surface fields above 1000-1200 nT a large portion of the surface was shielded from incident ions. However, for surface field strengths less than 800 nT, little deflection occurred and the surface flux was negligibly different from the incident flux. Since collective effects were ignored, the model underestimated the deflection of ions by the anomalies. It also focused on regions an order of magnitude smaller than the anomalous regions in the Imbrium and Serenitatis antipodes.

Previously, our knowledge of magnetospheres has been limited to large-scale structures produced by global magnetic fields. For planetary sized magnetospheres, particle interactions occur over a distance much smaller than the scale size of the magnetosphere. For a mini-magnetosphere, particle processes would be occurring on a range comparable to the scale size of the structure. Since these mini-magnetospheres are embedded in rock, the boundary acts solely as a sink for particles, whereas something like the Earth's ionosphere is both a sink and a source. Mini-magnetospheres are important as they can lead to localized structures that are much more dynamic, thereby providing crucial insight into solar wind-magnetospheric interactions and wave-particle heating interactions.

Two-dimensional numerical simulations provide a simple means to test for the formation of mini-magnetospheres and investigate changes in the macroscopic features of the mini-magnetosphere when the solar wind conditions are varied. Besides being a small-scale version of what we see around entire planets, mini-magnetospheres also have the potential to occur in a regime where the behavior of the plasma transitions from acting as individual particles to acting collectively as a fluid. It is not well understood exactly how and when that transition occurs and mini-magnetospheres could provide the laboratory to test theories. In this paper we will only discuss the predictions made from a fluid model. We have also run 2-D particle simulations that confirm the qualitative results from the fluid simulations. The results from the particle simulations will be published at a later time.

In order for the magnetized regions on the surface of the Moon to interact with the solar wind in such a way to form mini-magnetospheres, two minimum criteria must first be met. First, the field strength must be able to balance the dynamic pressure of the solar wind, and second, that balance must occur over a scale length larger than a proton gyroradius. For a solar wind number density of 1-20 protons/cm^3 with a velocity of 100-800 km/s, the minimum magnetic field required to balance the solar wind would be $\sim$ 7-230 nT, with a minimum magnetic field of 80 nT for the solar wind conditions of 10 particles/cm^3 and 400 km/s, the approximate solar wind conditions when LP saw a shock surface. For a magnetic field equal to the minimum for pressure balance and protons with $v_\perp$ equal to the solar wind velocity, the gyro-radius is 30-150 km (50 km for a minimum field of 80 nT). The regions on the Moon are above the lower limits but less than the upper end values. Therefore, for some solar wind conditions these approximations suggest that a shock can
form around the magnetic anomalies on the Moon.

If these regions of strong magnetic field found on the Moon do in fact form mini-magnetospheres, certain signatures should be present. An instrument traveling into a magnetosphere for an object such as the Earth first sees a large increase in density and pressure. As it enters the magnetosheath, the particles are slowed to subsonic speeds and the flow energy of the particles is converted into thermal energy, thus an increase in temperature of the particles occurs. At the magnetopause a large gradient in pressure and density is seen, and a current is present as well. A clear magnetic signature at the magnetopause is only present for southward IMF, when a change in the direction of B_z occurs. The two most

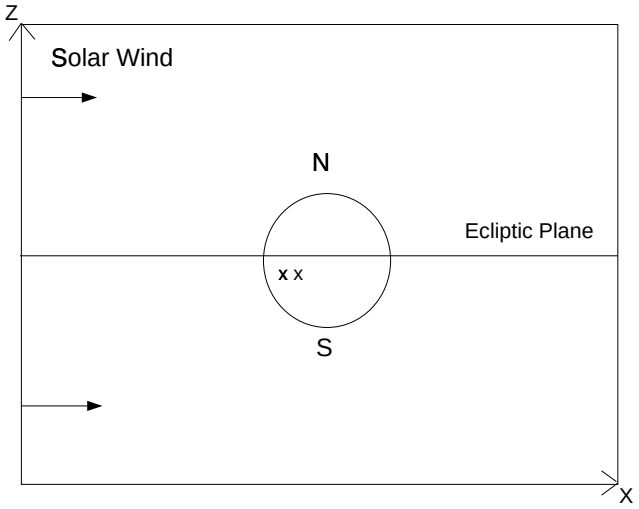

Figure 1. All of the following plots follow this convention. The arrows on the left-hand side indicate the direction of the solar wind. The line in the center of the box indicates the location of the ecliptic plane, with the north and south poles of the object above and below the plane. The two small crosses inside the object indicate the approximate location of the line currents for a dipole field with the moment in the $\pm\vec{z}$ direction. The vertical axis will be referred to as the $\vec{z}$ axis and the horizontal axis as the $\vec{x}$ axis.

prominent features seen from outside the shock are energized particles and plasma waves. These characteristics are investigated in the model described below.

2. Numerical Model of the Solar Wind at the Moon

The interaction of the solar wind with dipole magnetic fields located on the Lunar surface, in an MHD fluid approximation, can be simulated by a combination of fluid dynamic equations and Maxwell's equations [*Parks*, 1991,]. For our simulations, Ohm's law had the form

$$\mathbf{E} = -\mathbf{v} \times \mathbf{B}^{\rm tot} + \eta \mathbf{J}, \qquad (1)$$

where η is the scalar resistivity of the plasma.

For the 2-D simulations the electric field and current have components only in the third dimension, in and out of the simulation plane. In the results presented the direction away from the Sun is in the $\vec{x}$ direction and $\vec{z}$ is perpendicular to the ecliptic plane, the electric field and current are in the $\vec{y}$ direction. All other variables are constrained to the *xz* plane (Figure 1).

A two-step Lax-Wendroff process [*Richtmyer et al.,* 1967,] was used to solve the partial differential equations involving the mass density, the momentum, the magnetic field, and the energy of the plasma. All of these quantities were assumed to be continuous at the boundaries. After the two step Lax-Wendroff, Lapidus smoothing was used on the density, the momentum, and the energy to remove numerical instabilities that arise at discontinuities, such as the bow shock.

Faraday's and Ampere's law can be combined with Ohm's law to form the transport equation for the magnetic field:

$$\frac{\partial \mathbf{B}}{\partial t} = \nabla \times (\mathbf{v} \times \mathbf{B}) + \frac{\eta}{\mu_o} \nabla^2 \mathbf{B}. \qquad (2)$$

The first term on the right-hand side is the convection term, and the second term is the diffusion term. For an ideal MHD plasma, η = 0, but the error in the numerical solution of the magnetic field differential equation is of order $\alpha \nabla^2 \mathbf{B}$. Thus the numerical error will allow diffusion to still occur. The effective resistivity associated with the numerical diffusion is

$$\eta_{\rm num} = \frac{\mu_o}{2} \, \Delta t \, v_o^2, \qquad (3)$$

where Δt is the typical time step of the simulation and v_o is the typical Alfven speed. For these simulations the numerical resistivity was $\sim$ 0.15 ohm m.

The magnetic field needs to diffuse through the Moon though. This is done by setting the resistivity in (1) equal to zero everywhere except inside the object, where it was set to 10^4 ohm m. *Sonnet* [1975] placed the resistivity of the Lunar rock between 10^3 ohm m and 10^5 ohm m. The Reynolds number is the ratio of the convection term to the diffusion term and should be very large for diffusion to be negligible. For the simulations the magnetic Reynolds number was $\sim$ 0.43 inside the Moon, while the Reynolds number associated with the numerical resistivity was of the order of 56,000.

A nested-grid method was used for high resolution around the area of interest. The MHD equations were solved in all grids simultaneously. The values of the variables at points in the outer grid that overlap points in the inner grid, were replaced with the overlapping inner grid values. For internal grids the boundary values were set by the outer grid where points overlapped and interpolated values for the grid points where no overlap occurred. Three grids of 300 x 200 grid points were used with the spatial resolution equal to 34.8 km in the outer grid, 17.4 km in the middle grid, and 8.7 km in the innermost grid. The multiple box method allows for high resolution in a small area of interest without a substantial increase in computation time or complexity of code.

Simulations were run with the IMF set to 5 nT in the $\hat{x}$ direction or 2.5 nT in the $-\hat{z}$ direction. At these field strengths the IMF diffuses sufficiently fast through the Moon that there is no pile-up of IMF at the unmagnetized surface. For higher values, 3-D effects need to be incorporated to allow flow of

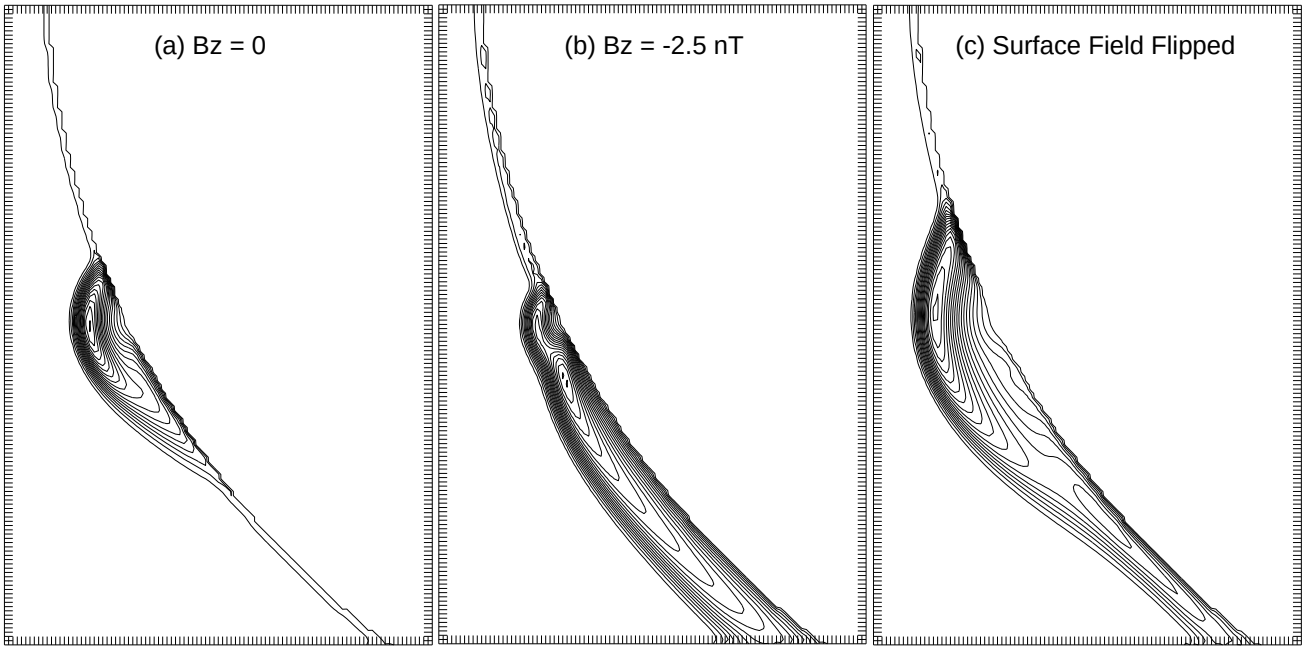

Figure 2. Pressure contours for three different initial conditions with a dipole located at 25^oS, measuring 30 nT at 100 km above the Lunar surface and 290 nT at the surface. The boxes correspond to a region 870.0 km by 1350.0 km, with the tick marks being units of 8.7 km. The solar wind is set to 10 ions/cm^3 with a speed of 400 km/s, and the surface pressure is held at a constant value of 5.5×10^{-7} nPa. Case a shows when the IMF is 5 nT parallel to the ecliptic plane with the surface field of the anomaly in the northward direction (dipole moment in $-\vec{z}$). The contour interval is 0.074 nPa. Case b and c are both for southward IMF of 2.5 nT. In case b the surface field points in the opposite direction as the IMF (dipole moment in $-\vec{z}$), whereas in case c the direction of the surface field was flipped to point in the same direction as the IMF, southward (dipole moment in $+\vec{z}$). The contour intervals for cases b and c are 0.083 and 0.089 nPa, respectively.

plasma and IMF around the flanks, and prevent an unphysical pile-up of IMF at the unmagnetized surface. Decreasing the conductivity of the Lunar surface increased the diffusion of the magnetic field through the surface, preventing pile-up of the IMF, as well as making the surface value more physical, but it also made the simulation unstable. MHD assumes infinity conductivity (zero resistivity) but can work for finite, but large conductivity. The conductivity of the Moon was set to the smallest value possible for which instability did not occur.

The average dayside ion density of the Lunar atmosphere was set at $10^{-1}\mathrm{cm}^{-3}$ and the nightside density $10^{-2}\mathrm{cm}^{-3}$ with an average molecular weight of 40 amu and scale height of $\sim$ 100 km [*Johnson*, 1971, ; *Hodges*, 1974,]. Ar^{40} constitutes the largest fraction of ions in the tenuous Lunar atmosphere, with only Neon becoming comparable during periods of extremely high solar flux. The model is a single species (proton) simulation; therefore the Lunar ionosphere had an effective number density of 4 ions/cm^3 on the dayside and 0.4 ions/cm^3 on the nightside. The ion temperature of the Lunar atmosphere is $\sim$ 400K [*Johnson*, 1971,] with the temperature of the solar wind $\sim 1.4 \times 10^5$ K. Thus the Lunar ionosphere acts as a sink for particles in the unmagnetized regions. The results are independent of variation in the actual values, so long as the atmosphere acts as a low-pressure region. The pressure and density cannot be set to zero though, as it would introduce division by zero into the numerical solutions.

Two line currents, oriented with opposing polarity, were used to create a dipole magnetic field at the equivalent of 25^oS. The line currents, separated by 13 km, were placed in a plane parallel to the ecliptic plane, 22 and 35 km below the surface, producing a dipole-like field with its effective dipole moment vector pointing north or south (Figure 1). A tilted dipole was created by moving one or both of the line currents off of the ecliptic plane. The magnetic field from line currents were used because they have unequal magnetic field strengths at the pole and equator. A 2-D dipole produces symmetric magnetic field strength. The magnitude of the magnetic field for a 3-D dipole is dependent on latitude, but the 3-D dipole formula can not be used with just one of the coordinates set to zero as that makes $\nabla \cdot \mathbf{B} \neq 0$. The strength of the field was set to 290 nT at the surface and the strength above the surface could be varied by the separation of the line currents. The maximum surface field was taken from the Lunar Prospector results since the large regions we are interested in would tend to average out the small pockets of much large field strength.

The initial conditions for each of the three cases focused on are listed in Figure 2. The orientation of the dipole moment, relative to the direction of the velocity of the solar wind, was also varied to determine its effect on the shape of the shock. The solar wind properties were initially set to a density of 10 protons/cm^3, with an speed of 400 km/s in the $\hat{x}$ direction.

3. MHD Results for Magnetic Anomalies on the Lunar Surface

No large-scale bow shock can be seen surrounding the entire Moon (Figure 2), as would be expected for a low-density and low-temperature object immersed in a hot solar wind. However, a shock, or mini-magnetosphere can be seen around the magnetized region for several solar wind and anomaly configurations, three of which are shown in detail. In large-scale magnetospheres two distinct boundaries occur, the first being the bow shock where the supersonic solar wind is slowed to subsonic speeds and the second occurring at the magnetopause where the pressure balance occurs between the solar wind dynamic pressure and the object's magnetic pressure. At the Earth's magnetopause a large change in the density and pressure occurs. A bow shock can be seen for all the mini-magnetospheres in Figure 2, but the inner boundary is much more complicated.

The definition of a magnetopause in the mini-magnetosphere is much more difficult since the internal structure is so compressed. A strict definition of the boundary between open and closed field lines does not have any of the typical signatures. There are no large gradients in pressure and density in the vicinity of the magnetopause. Instead, the pressure and density gradients constitute nearly all of the mini-magnetosphere. Rather than having two signature currents, one at the bow shock and one at the magnetopause, the increase in the magnitude of the current is a single structure, although the sign of the current can change within that region. Also, within a region 10-20 km thick around the magnetopause, the pressure, density, and temperature reach local maxima.

An expanded view of case A is shown in Figure 3 where the solar wind has a density of 10 protons/cm^3 and a speed of 400 km/s and an IMF of 5 nT in the ecliptic plane. The stand-off distance of the shock is $\sim$ 130 km on the outer edge, above the orbital height of Lunar Prospector. On the horizontal plane through the dipole location the pressure maximum occurs at $\sim$ 79 km above the surface and is 50 times the solar wind pressure, while the density reaches a maximum of 3.6 times the solar wind density at the same position. This position is also where the magnetopause occurs, as it is a region of transition to closed field lines and a current is present.

For points above and below the horizontal plane through the location of the dipole, the maximum values of pressure, density, and temperature decrease. The magnetic field at 100

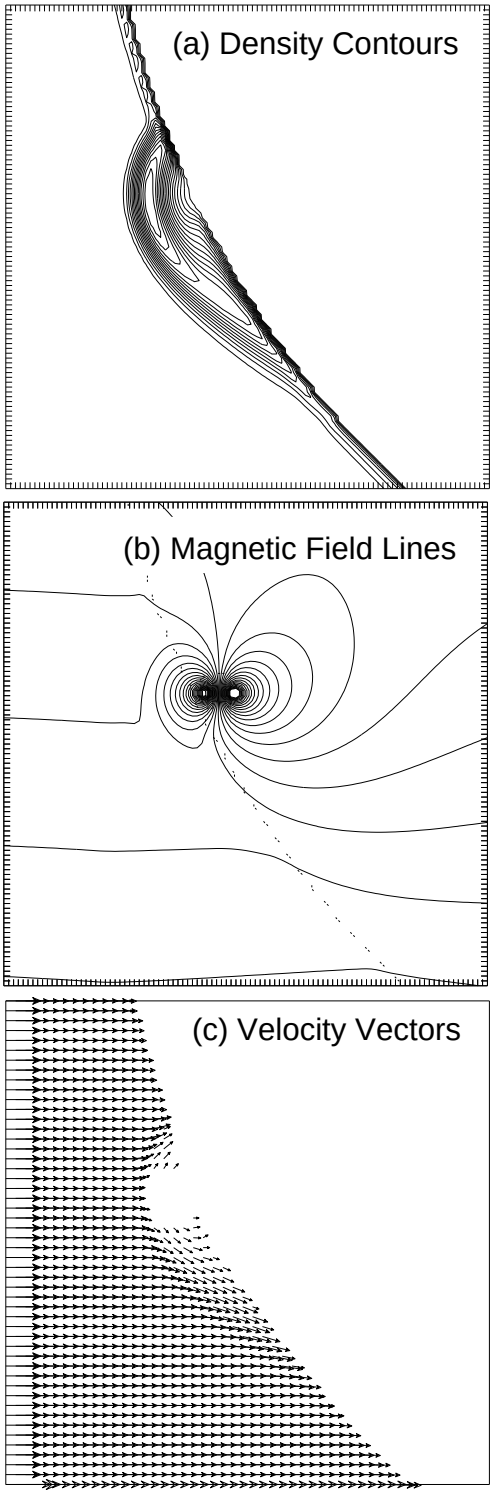

Figure 3. Case A: Magnified plots of density contours, magnetic field lines, and plasma flow for case a in Figure 2. The IMF is 5 nT in the ecliptic plane. Each tick mark equals 8.7 km, and the boxes contain a region 870 km by 870 km. The dotted line on the magnetic field line maps indicate the surface of the Moon. The contour interval for the density plot is 1.8 protons/cm^3. In all density plots the surface is at an effective constant density of 4.0 protons/cm^3 and the solar wind maintains a density of 10.0 protons/cm^3.

km above the dipole is just under 30 nT. Thus it is less than what the surface field was set to initially at that position and indicates that the dipole field has been compressed. The solar wind plasma slows due to the presence of the surface magnetic field and is deflected around the anomaly. Some plasma flows towards the anomaly in two cusp-like regions that separate open and closed field lines just above the surface.

The pressure and density maximum values are below the expected range for a solar wind with the Mach number of 10. The Rankine-Hugoniot conditions for a finite Mach number in the upstream region state that the density increase across a shock is by a factor of 5.7 and the pressure increases by a factor of over 100 for γ (the ratio of specific heats) equal to 1.4 [*Parks*, 1991,]. This assumes that the velocity normal to the shock inside the shock region is zero, and in all the cases examined, the flow is essentially all tangential.

The Rankine-Hugoniot conditions are for perpendicular shocks that are detached from the object. An oblique shock has jumps in density and pressure across the shock that are lower than in a perpendicular shock. Also, the close proximity of the shock to the cold surface of the Moon may cause the pressure increase to be smaller than expected for theory. For the cases analyzed the maximum increase in density and pressure is correlated to the size of the shock, with larger jumps seen for larger shocks.

Case B (Figure 4) has southward IMF of 2.5 nT, and the same solar wind conditions and dipole field strength as above. The IMF and the dipole field at the surface of the Moon are in opposite directions, allowing for dayside reconnection to occur. A shock surface still forms around the magnetic anomaly, but the stand off distance is only just over 100 km above the surface. The shock surface is also not spherical, as in case A; it is very elongated and has an indentation just below the plane containing the current elements that create the dipole. This indentation is in the same horizontal plane as a stagnation point. The elongation of the shock surface is due to the draping of the reconnected field lines, forming a mantle-like structure where the shocked plasma flows along the field lines around the Moon.

At the stagnation point the pressure and density increase to their global maxima but the temperature of the plasma does not. The maximum pressure and density occur $\sim$ 150 km south of the dipole and 61 km above the surface, while the maximum in temperature occurs 44 km directly above the location of the dipole. At the stagnation point the density increases to 4.5 times the solar wind density and the pressure increases to just under 60 times the pressure of the solar wind. At the location of the maximum in temperature the density only increase by a factor of 3 times the solar wind density and the pressure by a factor of 40. As in case A, these values are lower than predicted for a Mach number of 10.

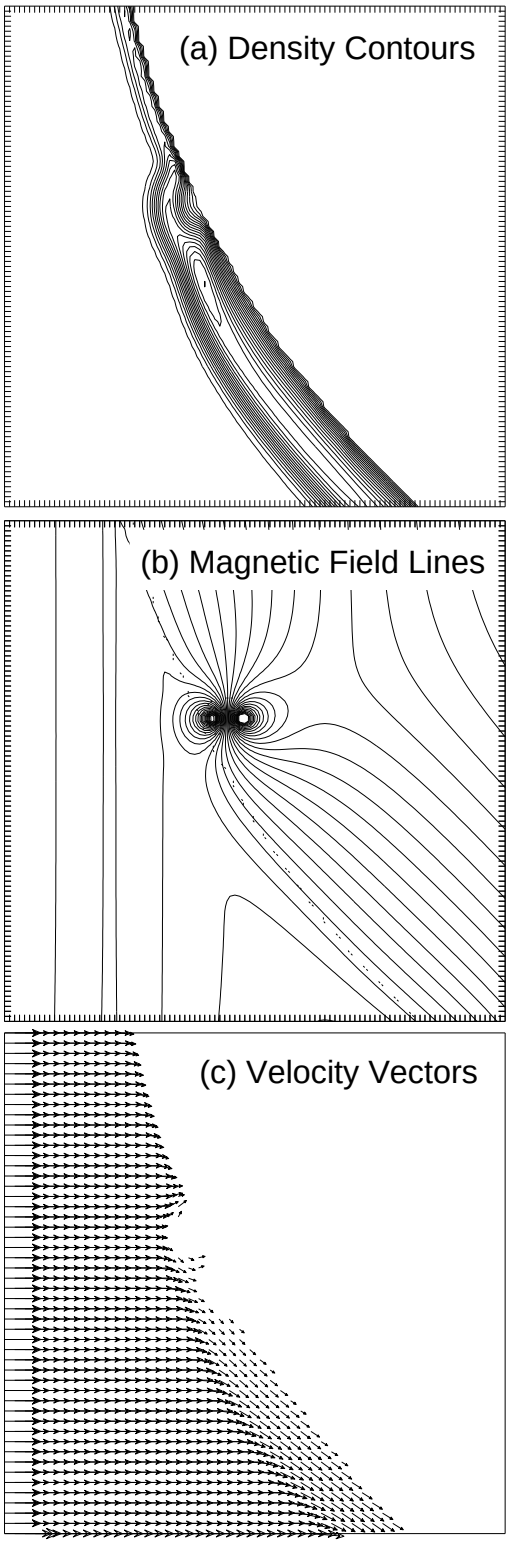

Figure 4. Case B: All parameters the same as in case A, except the IMF is 2.5 nT in the southward direction. All figures plotted on the same scale as those in Figure 3. The contour interval for the density plot is 2.2 protons/cm^3.

The plasma being deflected down by a simple obstacle should just flow around the Moon. Instead, in the present case it slows due to the reconnection of the IMF to the anomalous magnetic field, which forms kinked magnetic field lines. These kinked field lines appear to be causing the stagnation point, impeding the flow of plasma.

A substantial portion of the dipole field lines (Figure 4b) have reconnected to the IMF, eroding the surface field. As a result, the scale height of the magnetic field is seen to decrease such that the magnitude of the field at 100 km directly above the dipole is only 3 nT, with the magnetic field increasing to 30 nT at only 60 km above the surface, in the region around the dipole. The reconnected field lines allow an even more prominent flow of plasma into the cusp region for case B, than occurred in case A.

In case C (Figure 5) the direction of the dipole moment of the anomalous field was flipped so that the field at the surface is in the same direction as the IMF. This is analogous to flipping the direction of the IMF to northward in case B (the magnitude of both the IMF and the dipole remained the same). The shock surface is much rounder and moves out to 190 km directly above the dipole. In the case of Earth's magnetosphere, when the IMF change from southward to northward, the subsolar point moves out $\sim 1 - 2\ R_E$, or $\sim 10\%$ its distance from the Earth. In the case of the mini-magnetosphere the height of the bow shock above the Lunar surface changed by 90%.

A stagnation point below the dipole occurs in case C also, but unlike case B, the global maxima in pressure and density do not correspond to the location of the stagnation point. Rather, they were at the same location as the maximum temperature and the magnetopause, directly above the dipole. The spherical shape is due to what looks similar to a closed magnetosphere configuration in the Earth's magnetosphere. The IMF drapes around the magnetic anomaly, with much less reconnection of the dipole field to the IMF than in case B. The IMF piles up at the magnetopause, and the magnetic field line reconnection that does occur is in the interior of the Moon. As a result, the surface field is not nearly as eroded as it is in case B. At 100 km above the dipole, the total magnetic field is $\sim$ 50 nT, an order of magnitude increase from case B. Even though the mini-magnetosphere looks closed, the plasma near the surface and below the dipole can still flow into the cusp.

The falloff of the dipole field could be varied by changing the separation of the current elements generating the field. When the conditions in case A were varied such that the dipole strength was equal to 150 nT at the surface and 30 nT at 100 km above the surface (all other parameters remaining the same), the stand-off distance of the shock moved out to $\sim$ 200 km on the outer edge, an increase of $\sim 50\%$ from the

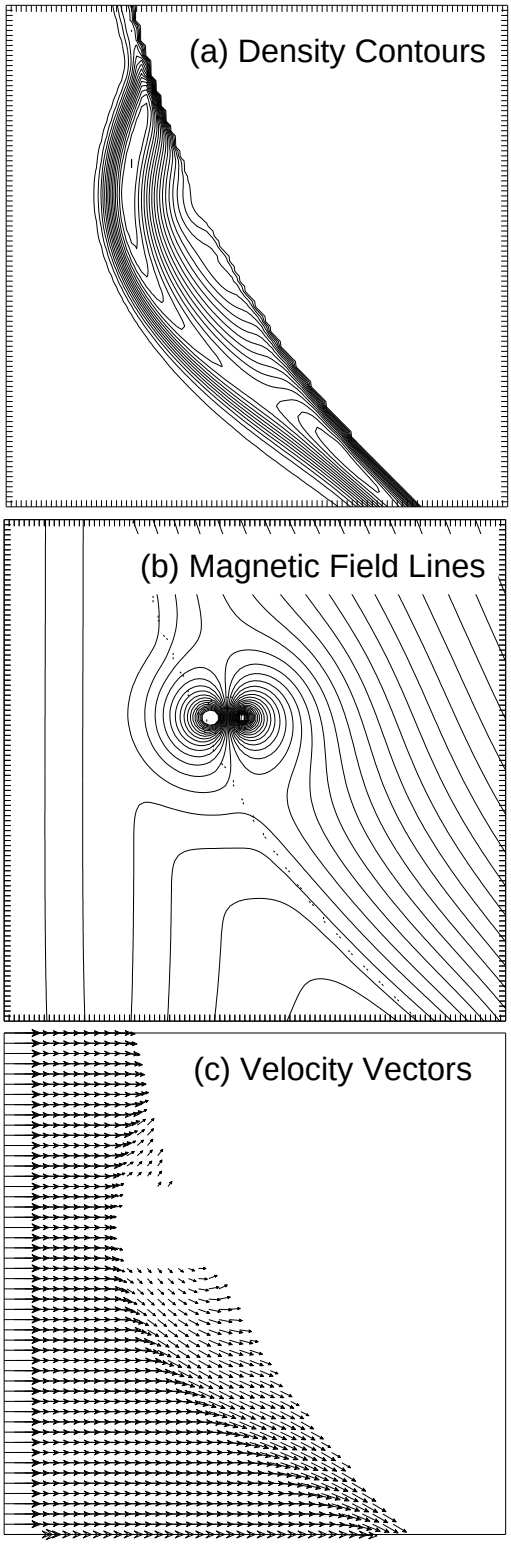

Figure 5. Case C: All parameters the same as in case B, except the dipole moment is flipped to the +z direction; thus the field at the surface is in the same direction as the IMF. This is analogous to flipping the IMF from southward to northward, for the same surface field. All figures plotted on the same scale as those in Figure 3 and 4. The contour interval for the density plot is also 2.2 protons/cm^3.

size in case A. The shape of the shock structure is the same as for case A, the overall size just increases. The total magnetic field at 100 km above the dipole is $\sim$ 20 nT, indicating some compression or erosion has occurred. When the surface field strength was set to 290 nT at the surface and 10 nT at 100 km above the surface, the mini-magnetosphere nearly disappeared. A very small mini-magnetosphere formed, but the outer edge was only $\sim$ 40 km above the surface.

When the ion density of the solar wind was decreased to $1/\mathrm{cm}^3$, in case A the outer edge of the shock surface formed at 260 km above the surface, for an initial anomalous field of 30 nT at 100 km and 290 nT at the surface. This is a 100% increase over the height of the shock surface from when the density is $10/\mathrm{cm}^3$ (all other parameters the same). For a low-density solar wind a stagnation point developed near the surface to the north of the anomalous region. Above the anomaly, the plasma is deflected into the inside surface shock, while below it is deflected down and around the Moon and is not impeded by kinked field lines. A low-density cavity also formed inside the shock region. The density reaches a maximum value of 4.5 ions/cm^3 at the magnetopause and then decreases to $\sim$ 2 ions/cm^3 in the region between the magnetopause and the surface of the Moon (which has an effective density of 4 ions/cm^3). A boundary in the pressure developed in the same location as well. This behavior is similar to that seen at the Earth's magnetopause.

The outer shock surface dropped to $\sim$ 35 km above the surface and no inner surface was visible, when the solar wind ion density was increased to $40/\mathrm{cm}^3$, for case A with the surface field set to 150 nT, and 30 nT at 100 km above the surface. When the velocity of the solar wind was decreased to 300 km/s, with the ion density remaining at $10/\mathrm{cm}^3$, a stagnation point developed and the outer surface moved out to $\sim$ 230 km, a 30% increase from the distance when the velocity of the solar wind plasma was 400 km/s.

When the conditions were the same as case C, except the IMF has components equal to 2.5 nT in both the $\vec{x}$ and $-\vec{z}$ directions, the mini-magnetosphere was nearly identical to the mini-magnetosphere in case C. This is similar to the Earth's magnetosphere, which tends to be insensitive to changes in B_x. In the simulations, when B_x is increased from 0 to 2.5 nT, the only changes are in the configuration of the open field lines and the location of the stagnation point.

4. Discussion

The cases focused on show that mini-magnetospheres can form for typical solar wind conditions, and while similar to the Earth's magnetosphere, there are substantial differences as well. The cases also highlight which parameters are the most important in determining the size and structure of a

mini-magnetosphere. The direction and strength of the IMF has the single greatest effect on the structure of the mini-magnetosphere for fixed lunar magnetic fields. Simply changing the direction of the IMF from South to North has nearly as big an effect on the size of the mini-magnetosphere as increasing the dynamic pressure of the solar wind by a factor of four. However, unlike increasing the dynamic pressure, flipping the direction of the IMF significantly changes the internal structure of the mini-magnetosphere as well. It caused the shock region to become very elongated, wrapping around the surface of the Moon.

However, changing the direction of the IMF, respective to the effective dipole moment, only produced large changes in the shape of the mini-magnetosphere when there was a significant component of the surface field in the same direction as the IMF, and the fluid flow was perpendicular to the IMF and dipole moment. This can be seen by comparing the large differences in case A and case B (Figure 2). The dipole moment of the surface field and the direction of the IMF are perpendicular in case A and parallel in case B, resulting in mini-magnetospheres that have a significantly different size and structure. However, when the angle between the dipole moment and the IMF rotated from perpendicular to anti-parallel (case A to case C), the size of the mini-magnetosphere increased, but the shape remained about the same. Also when the fluid flow, the IMF and the dipole moment were all parallel, the shape of the mini-magnetosphere was similar to those in case A and case C, with only the internal structure different. Varying the angle between the dipole moment vector and the IMF between 0^o and 90^o for IMF in the $\vec{x}$ direction did not cause the overall shape of the mini-magnetosphere to change dramatically, only the overall size and the location of the stagnation points inside the shock region changed. Thus the direction of the fluid flow relative to the IMF and surface field also contributes significantly to the shape of the mini-magnetosphere.

Changes in the magnitude of the solar wind velocity and density effect the size of the mini-magnetosphere, but not nearly as dramatically as some changes in the IMF. Changing the surface field strength had the least effect on size and shape, while varying the magnitude of the field at 100 km, when the surface field remained fixed, had a large effect on the resulting size of the mini-magnetosphere.

The above cases also indicate that the density and pressure increases predicted by the Rankine-Hugoniot conditions are an extreme upper bound, and the relative increase in density and pressure across the bow shock correlates with the size of the mini-magnetosphere. The largest jumps are seen in case C and for the conditions of case A but with low solar wind density (1 ion/cm^3). The maximal increases in density and pressure are by a factor of $\sim$ 4.5 and 65, respectively. The smallest increase is in case B, which also has the smallest scale size. This suggests that the closer a mini-magnetosphere forms to the Lunar surface, the more the magnetospheric plasma can be absorbed by the surface, reducing the buildup of plasma. Thus the predicted values from the Rankine-Hugoniot conditions are never reached, even for stagnation points.

We can test the validity of the MHD results by looking at the the size of the proton gyroradius in the mini-magnetospheres. The proton gyroradius at 100 km above the surface varied between 5 and 25 km inside the shock of the mini-magnetosphere in case C. In case B (the smallest mini-magnetosphere), the proton gyroradius at half way between the surface of the Moon and the shock surface ranged between 25 and 75 km. This places the plasma scale size close to the size of the mini-magnetosphere in some regions inside and indicates that in case B the MHD approximations are borderline in some regions.

Hood and Schubert [1980] showed that the charge separation that occurs at a magnetopause produces an electric field which reduces the necessary scale size for a magnetic anomaly to deflect the solar wind down to the geometric mean of the proton and electron gyroradii. For case B, where the size of the proton gyroradius inside the mini-magnetosphere suggests the MHD approximation may be breaking down, the scale size set by the geometric mean of the proton and electron gyroradii is $\sim 5 - 20$ km.

Hood and Schubert also showed that the length scale over which the magnetic field is nearly uniform is important for determining if a magnetic anomaly can deflect the solar wind. For a dipole-like field this scale length runs parallel to the dipole moment and is given by

$$L = B_z \ / \ \frac{\partial B_x}{\partial z} \tag{4}$$

for a dipole moment parallel to the *z* axis. For the solar wind conditions used in the simulation, with a field strength set to 290 nT at the surface and 30 nT at 100 km above the surface, $L \sim 176$ km. This size is significantly smaller than the lateral extent of the mini-magnetospheres presented above.

Preliminary 2-D particle simulations [*Harnett and Winglee*, 1999,] for conditions similar to the MHD simulations show that the anomalies are strong enough and large enough is size to hold off the solar wind and create a shock structure around the region. The particle simulations also show that the bow shock that forms can accelerate solar wind particles. Inside the shock region, the protons from the Lunar ionosphere can start to become demagnetized while the Lunar electrons remain strongly magnetized. This would lead to charge separation that cannot be modeled with a one fluid MHD simulation. The surface component of electrons form

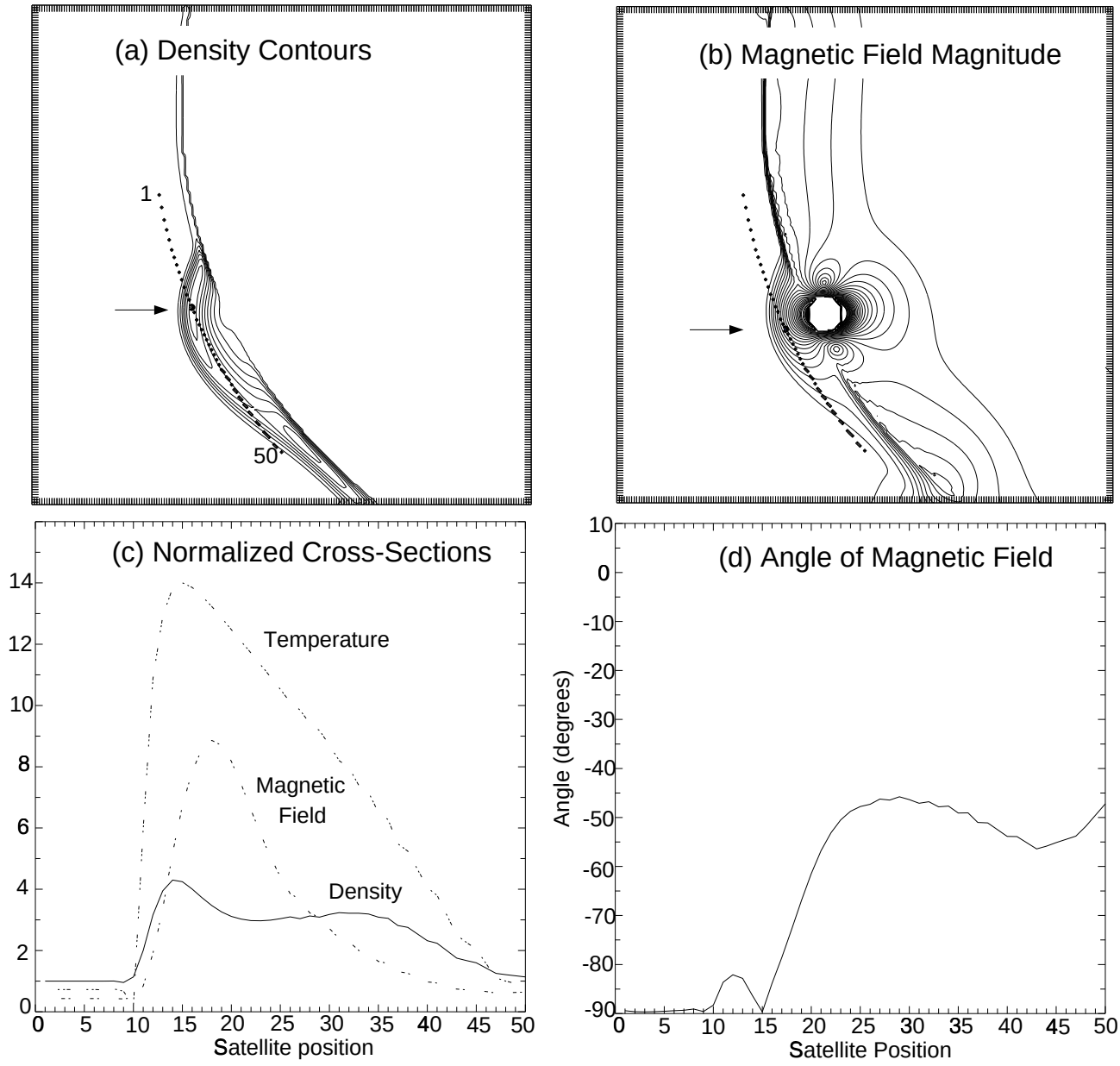

Figure 6. Cross-sectional cuts for a satellite orbiting at 100 km above the surface for the conditions in case C. The spots on Figures 6a and 6b indicate the positions that the data was sampled to create Figures 6c and 6d. The numbers on Figure 6a indicate the satellite positions plotted in Figures 6c and 6d. The contour interval for the density is 4.6 protons/cm^3, while the contour interval for the magnetic field is 6.1 nT, and both contain an area 1740 km by 1740 km, with the tick marks representing 8.7 km. The density, magnetic field magnitude, and temperature in Figure 6c are all in normalized units. The solid curve is the density, the curve composed of two dashed lines is the magnitude of the magnetic field, and the curve made with three dashed lines is the temperature. The normalizing constant is 10 protons/cm^3 for density, 5.79 nT for magnetic field, and 1.9×10^5 K for temperature. The angle of the magnetic field is measured relative to the ecliptic plane, with -90^o being the southward direction. The positions of the maxima in density and magnetic field in Figure 6c are marked in Figures 6a and 6b with horizontal arrows and an enlarged spot. The magnetic field Figure 6b was zeroed at the center of the dipole region for plotting purposes.

high-density regions inside the shock, similar to the structures seen in the MHD simulations. However, the surface proton densities, for some initial conditions, decrease in regions that surface electron densities increase. These results suggest that the MHD simulations are valid for predicting when a shock will form, and the size and general shape, but for smaller mini-magnetospheres, the internal structure of the ion population starts to deviate from a fluid behavior.

5. Characteristics of a Satellite Fly-by

Cuts can be taken through the data to mimic the trajectory of a satellite traveling at 100 km above the surface, just like Lunar Prospector (Figure 6). The maximum in density is encountered before the maximum in magnetic field. This is consistent with the measurements made by Lunar Prospector, where the increase in flux is seen before the increase in magnetic field. In the three cases detailed in Figures 2 - 5 the magnetic field begins to increase after the density. The simulations indicate that the contours of magnetic field magnitude follow the surface of the bow shock. This combined with the angle of the magnetic field lines suggests that the increase in magnetic field is due to both a combination of IMF pileup and compression of the surface field. There is not a clear transition between the two cases as there is in the Earth's magnetosphere. The transition region between pure IMF and closed field lines is only between 35 and 85 km wide, but it is $\sim$ 35 - 45$\%$ of the thickness of the mini-magnetosphere. In the Earth's magnetosphere the transition between open and closed field lines occurs primarily in the magnetosheath, which is over 2 R_E wide at the subsolar point (for a review, see *Kallenrode* [1998]), but the thickness of the region constitutes only $\sim$ 20$\%$ of the dayside magnetosphere.

During time interval when a shock region was reported over the Serenitatis antipode by LP [*Lin et al.*, 1998,], the solar wind ion density was $\sim$ 10/cm^3, while the solar wind speed slowly varied between 350 and 400 km/s. During the pass when the dynamic pressure of the solar wind increased, the ion density increased to 40/cm^3, while the average speed was just above 350 km/s. The simulations are consistent with the LP satellite, flying at an altitude near 100 km, first encountering the outer edge of a shock, where the pressure and density increase sharply, while the magnetic field increases more slowly. As the satellite approached a position directly above the magnetized region, it would have been traveling approximately tangential to the shock surface thus the pressure and density changed more slowly, while the magnitude of the magnetic field reached its maximum value. The pressure, density, and magnetic field then all decreased as the satellite traveled back out of the shock surface. Symmetry of the measurements about the maximum will depend on the location of the anomaly. Since the shock surface over the Serenitatis antipode is asymmetric, measurements of flux and magnetic field would be as well. When the solar wind pressure increased to 40/cm^3, as seen during the fourth orbit, the shock surface dropped so that only the outer edge would have been in the path of the satellite. Large-scale reconnection of the anomalous magnetic field to the IMF is consistent with the Lunar Prospector measurement of only small rotations in the magnetic field in the regions of increased magnitude.

The results are not completely consistent with the magnetic field measured by LP though. Magnetometer measurements made above the Serenitatis antipode, when the anomalous region was in the wake and the Moon was in the solar wind vary between 2 and 15 nT at 100 km (R. P. Lin,private communication, 1999). These values are comparable to the IMF as measured by the Wind satellite, indicating that the contribution due to the surface field is small compared to the IMF. For surface field strengths much less than 30 nT at 100 km, a shock would form in the simulations but significantly closer than 100 km above the surface. Also, as LP traveled through the shock region, the increase in magnetic field was from 10 to 30 nT, not the factor of 9 increased predicted by our model.

Three possibilities could explain the discrepancies. The first is the the 2-D nature of the simulations. 3-D dipole fields fall off faster than 2-D dipoles, so scaling the 3-D magnetic field down to 2-D requires increasing the strength of the magnetic field measured above the surface. Another possibility, and related to the first, is that the cumulative effects of the crustal magnetic fields in the entire Serenitatis antipode can not be accurately modeled with a simple dipole. The magnetized regions extend over hundreds of kilometers on a spherical surface, with plasma processes occurring relatively close to the source of the magnetic field. Also, it is possible that the boundary conditions at the surface of the Moon are not quite physical in the model. A magnetosheath-like region occurs where the temperature of the plasma increases by an order of magnitude when crossing the bow shock. The largest temperatures occur 50 to 100 km above the surface, which may induce significant heating at the surface. The simulations were run with the surface of the Moon held fixed to its cold 400 K. Including heating at the surface in the anomalous region could inflate the shock surface and allow the much smaller field strengths seen by LP to create mini-magnetosphere with a much larger scale size.

6. Conclusion

The results from MHD simulations indicate that Lunar Prospector did in fact encounter a mini-magnetosphere. Mak-

ing predictions about the properties of a mini-magnetosphere is not just a matter of scaling down an Earth-sized magnetosphere due to the small scale size and the boundary conditions of the material the anomalies may be embedded in. The simulations suggest that a mini-magnetosphere will form when the anomalous magnetic field of 290 nT at the surface is greater than 10 nT at 100 km above the surface, for solar wind of 10 ions/cm^3 traveling at 400 km/s. For an anomalous field of 30 nT at 100 km above the surface, a mini-magnetosphere will form when the solar wind density was less than 40 ions/cm^3. The magnitude of real anomalous magnetic fields has not been measured to be anywhere near 30 nT at 100 km above the surface (a typical value at 100 km above the surface is 2 nT), but scaling the 2-D magnetic field up to 3-D would cause the field above the surface to fall off faster. 3-D simulations would also allow for a more realistic model of the surface source. The real magnetic anomalies should be modeled with multiple dipoles in the 700 - 1000 km diameter regions of magnetization at the Imbrium and Serenitatis antipodes. Therefore, in 3-D a field strength smaller than 30 nT at 100 km could still hold off the solar wind.

The mini-magnetospheres that formed contained both a bow shock and magnetopause. However, the large gradient in the pressure and density that is seen at the Earth's magnetopause is not present at the magnetopause occurring around the anomalies. Instead, the size of the boundary layers are on the order of the mini-magnetosphere itself. The magnetopause of a mini-magnetosphere has the characteristic that the pressure, density, temperature, and magnitude of the current all reach local maxima.

Most of the cases in the study also have stagnation points, places where the density and pressure increase but the temperature does not. Two mechanisms appear to cause the stagnation points. In the region to the north of the dipole where the bow shock contacts the Lunar surface, the plasma is deflected up into inner edge the shock surface. For some solar wind/anomaly configurations the pressure and density could build up forming a stagnation point. The plasma that is deflected down, in most cases flows around the object unimpeded. However, reconnection can cause a stagnation point to develop in this region as well. The open field lines can be kinked, impeding the flow of plasma.

Cuts though the mini-magnetosphere show that the increase in magnetic field is due to a combination of a pile-up of the IMF and compression of the surface field, with no clear transition between the two as there is in the Earth's magnetosphere. However, structures that look very similar to the Earth's cusps occur in the mini-magnetospheres. The cusp-like regions occur in the region between closed and open field lines and plasma can flow to the surface through them.

Because the plasma processes are on a scale comparable to the size of the mini-magnetosphere, small changes in some parameters can have a dramatic affect on the properties of the mini-magnetosphere. The IMF conditions had greatest impact on the size and internal structure of the mini-magnetosphere. Just the equivalent of changing the IMF from southward to northward caused a 90% increase in the size of the mini-magnetosphere. Also the change is not just the stand-off distance from the surface. The shape of the mini-magnetosphere is highly dependent on the the IMF orientation, ranging from semicircular to very flat and elongated, depending on the location of reconnection. However, this dramatic change only occurred when the flow of the plasma was perpendicular to the direction of the IMF and effective dipole moment of the surface source, while the IMF and dipole moment were parallel. Changes in the solar wind dynamic pressure and the surface field strength change the mini-magnetosphere but generally only effect the size, not the shape or internal structure. Also decreasing the strength of the anomalous region above the surface, while holding the surface strength fixed, caused the size of the mini-magnetosphere to decrease significantly.

The next step in the research will be to run three dimension simulations for both the Moon and Mars. A 3-D simulation will allow for the investigation of the cumulative effects of the crustal magnetization over the full Lunar surface. The combination of interactions between different mini-magnetospheres and different magnetic anomalies should produce a highly structured environment, whose dynamics may be even more dependent on variations in the solar wind conditions. Magnetic anomalies have recently been discovered on the surface of Mars, but with average scale sizes of the order of the largest Lunar anomaly and average magnetic field strengths 3 times larger than the largest surface magnetic field measured by Lunar Prospector. The 3-D simulations for the Moon will be extended to predict the effect that magnetic anomalies on the surface of Mars will have on the shape and location of the bow shock and ionopause, as well as determining how the anomalous field interacts with the IMF. The asymmetry of the anomalous region in conjunction with the rotation of the planet could cause the transport of particles in the downstream region of the Martian magnetosphere to be significantly different than those process in the Earth's magnetosphere. A particle tracker will also be employed to investigate how the small scale size effects the particle interactions with the mini-magnetospheres. Comparing the MHD results with the particle simulations for this small scale may also help in studying how the individual plasma particles begin to act collectively as a fluid.

Acknowledgments.

This work was funded by NSF grant ATM-9731951 and NASA grants 61-9801 and 62-1693. Janet G. Luhmann thanks Lon L. Hood and another referee for their assistance in evaluating this paper.

References

Dyal, P., et al., Magnetism and the interior of the Moon, *Rev. Geophys., 12,* 568-591, 1974.

Harnett, E.M., and R.M. Winglee, Two dimensional simulations of the solar wind interaction with magnetic anomalies on the surface of the Moon, *Eos Trans. AGU, 80*(17), Fall Meet. Suppl., F873, 1999.

Hodges, R.R., The lunar atmosphere, *Icarus, 21,* 415-426, 1974.

Hood, L.L., and G. Schubert, Lunar magnetic anomalies and surface optical properties, *Science, 208,* 49-51, 1980.

Hood, L.L., and C.R. Williams, The lunar swirls: Distribution and possible origins, *Proc. Lunar Planet. Sci. Conf., 19th,* 99-113, 1989.

Hood, L.L., et al., Contour maps of lunar remanent magnetic fields, *J. Geophys. Res., 86,* 1055-1069, 1981.

Johnson, F.S., Lunar atmosphere, *Rev. Geophys., 9,* (3), 813-823, 1971.

Kallenrode, M.-B., *Space Physics,* Springer-Verlag, New York, 1998.

Lin, R. P., et al., Lunar surface magnetic field concentrations antipodal to young large impact basins, *Icarus, 74,* 529-541, 1988.

Lin, R. P., et al., Lunar surface magnetic fields and their interaction with the solar wind: Results from Lunar Prospector, *Science, 281,* 1480-1484, 1998.

Parks, G., *Physics of Space Plasmas,* Addison Wesley, Readwood City, Calif., 1991.

Richtyer, R.D, and K.W. Morton, *Difference Methods for Initial Value Problems,* Interscience, New York, 1967.

Russell, C.T., and B.R. Lichtenstein,On the source of lunar limb compression, *J. Geophys. Res., 80,* 4700-4711, 1975.

Sharp, L. R., et al., Orbital mapping of the lunar magnetic field, *Moon, 7,* 322-341, 1973.

Sonnet, C.P., Solar wind induction and lunar conductivity, *Phys. Earth Planet. Inter., 10,* (3), 313-322, 1975

E. Harnett and R. Winglee, Geophysics Program, Box 351650, University of Washington, Seattle, WA 98195-1650. (eharnett@geophys.washington.edu; winglee@geophys.washington.edu)

Received March 6, 2000; revised August 3, 2000; accepted August 3, 2000.

Figure 1. All of the following plots follow this convention. The arrows on the left-hand side indicate the direction of the solar wind. The line in the center of the box indicates the location of the ecliptic plane, with the north and south poles of the object above and below the plane. The two small crosses inside the object indicate the approximate location of the line currents for a dipole field with the moment in the $\pm\vec{z}$ direction. The vertical axis will be referred to as the $\vec{z}$ axis and the horizontal axis as the $\vec{x}$ axis.

Figure 2. Pressure contours for three different initial conditions with a dipole located at 25^oS, measuring 30 nT at 100 km above the Lunar surface and 290 nT at the surface. The boxes correspond to a region 870.0 km by 1350.0 km, with the tick marks being units of 8.7 km. The solar wind is set to 10 ions/cm^3 with a speed of 400 km/s, and the surface pressure is held at a constant value of 5.5×10^{-7} nPa. Case a shows when the IMF is 5 nT parallel to the ecliptic plane with the surface field of the anomaly in the northward direction (dipole moment in $-\vec{z}$). The contour interval is 0.074 nPa. Case b and c are both for southward IMF of 2.5 nT. In case b the surface field points in the opposite direction as the IMF (dipole moment in $-\vec{z}$), whereas in case c the direction of the surface field was flipped to point in the same direction as the IMF, southward (dipole moment in $+\vec{z}$). The contour intervals for cases b and c are 0.083 and 0.089 nPa, respectively.

Figure 3. Case A: Magnified plots of density contours, magnetic field lines, and plasma flow for case a in Figure 2. The IMF is 5 nT in the ecliptic plane. Each tick mark equals 8.7 km, and the boxes contain a region 870 km by 870 km. The dotted line on the magnetic field line maps indicate the surface of the Moon. The contour interval for the density plot is 1.8 protons/cm^3. In all density plots the surface is at an effective constant density of 4.0 protons/cm^3 and the solar wind maintains a density of 10.0 protons/cm^3.

Figure 4. Case B: All parameters the same as in case A, except the IMF is 2.5 nT in the southward direction. All figures plotted on the same scale as those in Figure 3. The contour interval for the density plot is 2.2 protons/cm^3.

Figure 5. Case C: All parameters the same as in case B, except the dipole moment is flipped to the +z direction; thus the field at the surface is in the same direction as the IMF. This is analogous to flipping the IMF from southward to northward, for the same surface field. All figures plotted on the same scale as those in Figure 3 and 4. The contour interval for the density plot is also 2.2 protons/cm^3.

Figure 6. Cross-sectional cuts for a satellite orbiting at 100 km above the surface for the conditions in case C. The spots on Figures 6a and 6b indicate the positions that the data was sampled to create Figures 6c and 6d. The numbers on Figure 6a indicate the satellite positions plotted in Figures 6c and 6d. The contour interval for the density is 4.6 protons/cm^3, while the contour interval for the magnetic field is 6.1 nT, and both contain an area 1740 km by 1740 km, with the tick marks representing 8.7 km. The density, magnetic field magnitude, and temperature in Figure 6c are all in normalized units. The solid curve is the density, the curve composed of two dashed lines is the magnitude of the magnetic field, and the curve made with three dashed lines is the temperature. The normalizing constant is 10 protons/cm^3 for density, 5.79 nT for magnetic field, and 1.9×10^5 K for temperature. The angle of the magnetic field is measured relative to the ecliptic plane, with -90^o being the southward direction. The positions of the maxima in density and magnetic field in Figure 6c are marked in Figures 6a and 6b with horizontal arrows and an enlarged spot. The magnetic field Figure 6b was zeroed at the center of the dipole region for plotting purposes.